Multiphase models for moving boundary problems in biology

Ishraq U. Ahmed, Jennifer A. Flegg, Claire Miller, Ricardo Ruiz-Baier, Joshua Won, and Adriana Zanca

Abstract We address the modelling of tissue deformation using mixture theory. The governing equations consist of mass and momentum balances for two phases, and are written in Eulerian and Lagrangian frameworks using an active stress approach. We specify the general formulation for relatively simple representative examples in the context of tumour growth and early stages of atherosclerotic plaque development.

1 Introduction

Our current understanding of both the physiological and pathological conditions under which tissue growth and development occurs remains incomplete. In this work we explore the process of tissue growth: the addition of mass to the tissue through

————————————————

Ishraq U. Ahmed
School of Mathematics and Statistics, University of Sydney, Camperdown 2006 NSW, Australia
e-mail: `ishraq.uddin@sydney.edu.au`

Jennifer A. Flegg
School of Mathematics and Statistics, University of Melbourne, Parkville 3052 VIC, Australia
e-mail: `jennifer.flegg@unimelb.edu.au`

Claire Miller
Auckland Bioengineering Institute, The University of Auckland, Auckland 1010, New Zealand
e-mail: `claire.miller@auckland.ac.nz`

Ricardo Ruiz-Baier
School of Mathematics, Monash University, 9 Rainforest Walk, Clayton 3800 VIC, Australia
e-mail: `ricardo.ruizbaier@monash.edu`

Joshua Won
School of Mathematics and Statistics, University of Sydney, Camperdown 2006 NSW, Australia
e-mail: `joshua.won@sydney.edu.au`

Adriana Zanca
School of Mathematics and Statistics, University of Melbourne, Parkville 3052 VIC, Australia
e-mail: `a.zanca@student.unimelb.edu.au`

cell growth and rearrangement without changing its mechanical properties. Tissue growth is observed in several biological processes including remodelling and morphogenesis [31]. In many biological contexts, for example avascular tumour growth, external nutrients diffuse into the tumour providing sufficient energy for the tumour cells to proliferate [17]. There are multiple approaches to modelling these phenomena, from cell-based models to large-scale continuum models including high-order phase-field frameworks [26, 27, 35]. The purpose of this research project is to explore a configuration of multiphase models in general geometries, where the specific physical and geometrical characteristics of individual cells are not considered but rather each point in space is regarded as occupied by a particle belonging to each constituent (coexisting continua). As specific biological applications of this framework, we consider two phenomena: tumour growth and atherosclerotic plaque formation. We note that this framework can also be applied to other biological contexts such as chemotactic cell aggregates [22]. We build on the Eulerian two-phase model for avascular tumour growth described in [9] which considers two phases: viscous tumour cells and inviscid interstitial extracellular fluid. We extend this from a single dimension to general geometries then pull-back the set of equations to their Lagrangian counterpart. The active deformation of tissue (which encodes the growth process in the model) is represented using the active stress approach (also known as additive split of forces) [2].

Finding closed-form solutions to the nonlinear coupled problems discussed above is only possible in very restricted scenarios and simplified settings. We opt for solving the governing equations numerically. The numerical framework undertaken here uses the method of lines, adopting a backward Euler scheme for the discretisation in time and finite element methods in space using a total Lagrangian approach. This method has been used extensively for growth modelling (see for example [28, 31]). Here we derive a formulation which is consistent with the multiphase poromechanical description. The specific form of the resulting system of equations (in the Lagrangian setting) has as unknowns the displacement of the first phase, the pressure of the second phase, the nutrient (oxygen) tension, and the volume fraction of the first phase. We adopt a monolithic method that requires stable mixed element pairs (in the sense of the Babuška–Brezzi theory [8]) for the approximation of displacement and volume fraction. For the problem at hand, using the MINI element (piecewise linear displacements enriched with cubic bubble functions and piecewise linear and continuous elements for volume fraction) is efficient and sufficiently accurate, but other techniques including stabilisation of low-order schemes with discontinuous volume fractions [6] or mixed methods based on the Hu–Washizu three-field variational principle [34], could be employed in cases where high gradients of the volume fraction are expected and when the material parameters approach the incompressibility limit.

Understanding the mechanisms of moving boundaries in the applications addressed herein can contribute to gaining insight on tissue characterisation, the design and optimisation of medical devices, and the personalisation of surgical and pharmacological medical treatment.

In Section 2 we present a mixture theory model for tumour growth, addressing its extension to the Lagrangian framework and its finite element discretisation. Section 3 contains the derivation of a new model for the early stages of atherosclerosis (more specifically, regarding plaque formation). We continue the theory of mixtures, but the active mechanisms in the plaque formation are concentrated on interfacial fluxes. We write a simplified model valid in the axisymmetric case. In Section 4 we close with a discussion on the limitations of our study and explore possible extensions.

2 A general multiphase tumour model in general geometries

Tumour growth has long been an area of considerable interest to the mathematical biology community. In addition to the devastating impacts tumours can have on individuals and the healthcare system, tumour growth is a process that is amenable to mathematical studies. Early stage tumour growth - such as that we are considering here - is often avascular, in other words, it does not involve blood vessels. Avascular tumours are simpler to model, since interactions with and development of vasculature are not considered. In the early 1970's, Greenspan developed a continuum, compartmental model for avascular tumour growth that is still expanded upon and used for comparison today [23, 24, 36]. In contrast, Landman and Please [32] developed a mixture model of cells and extracellular water and proposed that the differing pressures in each phase drive tumour behaviour. Subsequent tumour models have utilised the mixture model framework, extending and refining earlier assumptions [9–11,13,33,37]; for comprehensive reviews on modelling of avascular tumour growth, refer to [4,12,38]. One such model is that proposed by Breward *et al.* [9]. In their model, the cellular phase behaves similarly to viscous fluid, and the extracellular phase is assumed to be inviscid. Furthermore, the development of the necrotic core of the tumour depends on oxygen tension. In this section we generalise Breward *et al.*'s model to general geometries, and then numerically solve the system in the two-dimensional case for two different geometries. We note that alternative approaches to solving two and three-dimensional multiphase avascular and vascular tumour models are possible [16–18, 25, 43].

2.1 Governing equations in Eulerian form

We derive here a set of governing equations starting from the main assumption that a given biological tissue is a medium composed by a solid phase (containing cells of diverse types) and an interstitial fluid completely filling the void spaces. For this we consider the two phase model from [9] and continue the basic assumptions held in their model; that there are no voids such that

$$\alpha + \beta = 1, \tag{1}$$

where α and β represent the (dimensionless) volume fractions of the two phases. We also assume that mass and momentum are conserved. We redefine these initial equations to general geometries, where the mass balance equations in each phase become:

$$\frac{\partial \alpha}{\partial t} + \nabla_x \cdot (u_\alpha \alpha) = q_\alpha, \tag{2a}$$

$$\frac{\partial \beta}{\partial t} + \nabla_x \cdot (u_\beta \beta) = q_\beta, \tag{2b}$$

where u_α and u_β denote the velocities of their respective phases, while q_α and q_β denote the respective net production rates of tumour cells and fluid. The x-subindex indicates that the spatial derivatives are taken with respect to the Eulerian coordinates.

The momentum balance equations become:

$$\nabla_x \cdot (\alpha \sigma_\alpha) + f_\alpha = 0, \tag{3a}$$
$$\nabla_x \cdot (\beta \sigma_\beta) + f_\beta = 0. \tag{3b}$$

Here σ_α and σ_β are the respective Cauchy stresses and f_α and f_β are the respective net sources of momentum. We set

$$
\begin{aligned}
\sigma_\alpha &= -p_\alpha \mathbf{I} + 2\mu_\alpha \varepsilon(u_\alpha) + \lambda_\alpha (\nabla_x \cdot u_\alpha) \mathbf{I}, \quad & \sigma_\beta &= -p_\beta \mathbf{I}, \\
f_\alpha &= p_\beta \nabla \alpha + \kappa \alpha \beta (u_\beta - u_\alpha), & f_\beta &= p_\beta \nabla \beta - \kappa \alpha \beta (u_\beta - u_\alpha),
\end{aligned}
\tag{4}
$$

where $\varepsilon(u_\alpha) = \frac{1}{2}(\nabla_x u_\alpha + \nabla_x u_\alpha^T)$ is the strain rate tensor, μ_α and λ_α are the shear and bulk viscosities respectively for the cell phase, and p_α and p_β are the respective average pressures. The net momentum sources contain a drag term accounting for the relative motion of the two phases, and an interfacial force coupling pressure with the gradient of volume fraction. The drag coefficient is denoted by κ. We define Σ_α to encode a capillary pressure (the difference between the pressures in the two phases) $\Sigma = p_\alpha - p_\beta$, and it is assumed to have the following form (depending on α)

$$\Sigma(\alpha) = \begin{cases} \gamma \dfrac{\alpha - \alpha^*}{(1-\alpha)^2} & \text{if } \alpha > \alpha_{\min}, \\ 0 & \text{if } \alpha < \alpha_{\min}. \end{cases} \tag{5}$$

Based on our assumptions, it also follows that $q_\alpha = -q_\beta$, reflecting conservation of mass for the cell-fluid mixture. Moreover, $f_\alpha = -f_\beta$, reflecting that no external forces act upon the cell-fluid mixture.

The source/sink terms are assumed to be dependent on the concentration of an externally supplied nutrient, here taken to be oxygen. The functional form of q_α is defined to agree with [40]

$$q_\alpha(\alpha, C) = \frac{(1+s_1)\alpha(1-\alpha)C}{(1+s_1 C)} - \frac{s_2 + s_3 C}{1+s_4}\alpha, \tag{6}$$

where s_i, $i \in \{1,2,3,4\}$, are constants and the oxygen tension is denoted by C. The positive and negative terms in the equation for q_α correspond to cell division and death, respectively. The factor $(1-\alpha)$ in the cell division term indicate that the growth rate decreases together with the available space.

Due to the separation of time–scales between the cell dynamics and nutrient transport (the timescale of tumour cell proliferation is typically much longer than that of oxygen diffusion), we simply describe oxygen dynamics by

$$-\nabla_x^2 C = q_C(\alpha, C), \tag{7}$$

where Δ is the Laplacian operator, and the reactive term assumes the following specification

$$q_C(\alpha, C) = -\frac{Q\alpha C}{1 + \hat{Q}_1 C}, \tag{8}$$

where Q represents the scaled oxygen consumption rate (scaled by the oxygen diffusion coefficient), and the positive constant $\hat{Q}_1$ describes how fast the tumour cells consume oxygen as oxygen levels change.

Based on the above considerations, a mass conservation equation and a momentum balance for the mixture can be derived by summing up (2a) and (2b), and (3a) and (3b), respectively. This leads to the following set of equations, all written in an Eulerian frame:

$$\frac{\partial \alpha}{\partial t} + \nabla_x \cdot (u_\alpha \alpha) = q_\alpha(\alpha, C), \qquad \text{continuity of phase } \alpha$$

$$\nabla_x \cdot \left(u_\alpha - \frac{(1-\alpha)}{\kappa\alpha}\nabla p_\beta \right) = 0, \qquad \text{continuity of the mixture}$$

$$-\nabla_x \cdot (\sigma) = 0, \qquad \text{momentum balance}$$

$$\sigma = -\alpha\Sigma(\alpha)\mathbf{I} - p_\beta \mathbf{I} + 2\alpha\mu_\alpha\varepsilon(u_\alpha) + \lambda_\alpha(\nabla_x \cdot u_\alpha)\mathbf{I},$$

$$\qquad \text{constitutive equation}$$

$$-\nabla_x^2 C = q_C(\alpha, C). \qquad \text{continuity of oxygen}$$

Note that the conservation of angular momentum reads $\sigma^T = \sigma$, and note also that effective unknowns of the problem are the viscous fluid (cell) volume fraction α, the viscous fluid (cell) velocity u_α, the fluid pressure p_β, and the oxygen tension C.

We have considered the above equations in the current configuration Ω (which depends on t) with coordinates x. This system of equations in general coordinates coincides with the one derived in [17].

2.2 Governing equations in Lagrangian form

To circumvent the need of solving the set of equations in a moving domain, the goal in this section is to re-define the problem in Lagrangian coordinates. The motion of material points in a body that occupies region Ω_0 with boundary $\partial\Omega_0$ in the initial state, moves to region Ω with boundary $\partial\Omega$ in the current state. The motion map can be characterised by a $\mathscr{C}^1$ (and bijective) vector field (the deformation or motion map)

$$\chi : \Omega_0 \to \Omega, \qquad \mathbf{X} \mapsto \chi(\mathbf{X}) = x(\mathbf{X},t) \qquad \text{for all } \mathbf{X} \in \Omega_0,\ t \in \times(0,T],$$

and we have that $\chi^{-1}(x,t) = \mathbf{X}$ for all $x \in \Omega$.

The material time derivative $\frac{D}{Dt}$ (with respect to a fixed material coordinate $\mathbf{X}$) for a scalar function $\phi(x(\mathbf{X},t),t)$, defined by applying the chain rule for differentiation, is:

$$\frac{D\phi}{Dt} = \frac{D\phi}{Dt}\bigg|_{\mathbf{X}} = \frac{\partial\phi}{\partial t} + \nabla_x\phi \cdot \frac{\partial x}{\partial t} = \frac{\partial\phi}{\partial t} + \nabla_x\phi \cdot u.$$

We consider a displacement field $d : \Omega_0 \to \Omega$. This displacement is associated with the deformation map χ such that

$$\begin{aligned} x &= \chi(\mathbf{X}) \\ &= \mathbf{X} + d \text{ where } d \text{ is the displacement.} \end{aligned} \tag{9}$$

The tensor $\mathbf{F}$ is the gradient of the deformation map such that

$$\mathbf{F} = \nabla_{\mathbf{X}}\chi = \mathbf{I} + \nabla_{\mathbf{X}}d, \tag{10}$$

and the Jacobian of the transformation representing local change of volume is

$$J(\mathbf{X},t) = \det\mathbf{F}(\mathbf{X},t).$$

For the two configurations Ω and Ω_0, we denote the outward unit normals of the respective domains as n and $\mathbf{N}_0$, related through $n = \mathbf{F}^{-T}\mathbf{N}_0$, where we have used the notation $\mathbf{F}^{-T} = (\mathbf{F}^{-1})^T$. Understanding ds and ds_0 as spatial differences in the respective domains and dV and dV_0 as current and initial volume elements, we recall the relation

$$J\,dV_0 = dV, \tag{11}$$

and Nanson's formula

$$J\mathbf{F}^{-T}\mathbf{N}_0\,dS_0 = n\,ds. \tag{12}$$

From the Eulerian momentum balance for the fluid phase (3b) we can obtain the following relation (corresponding to Darcy's law, see, e.g., [15])

$$\frac{1-\alpha}{\alpha\kappa}\nabla_x p_\beta = (1-\alpha)(u_\alpha - u_\beta). \tag{13}$$

Using the Maxwell principle for transport and localisation, (13) can be rewritten in the undeformed domain in the following form

$$J\frac{1-\alpha}{\alpha\kappa}\mathbf{F}^{-1}\mathbf{F}^{-T}\nabla_{\mathbf{X}} p_\beta = J(1-\alpha)\mathbf{F}^{-1}(u_\alpha - u_\beta). \tag{14}$$

The mass balance for α (2a), becomes, in Lagrangian coordinates

$$\frac{D}{Dt}(\alpha J) = J q_\alpha \qquad \text{in } \Omega_0 \times (0, T], \tag{15}$$

whereas for β we use the generalised Reynolds theorem together with (14) to arrive at

$$\frac{D}{Dt}(\beta J) - \nabla_{\mathbf{X}} \cdot (J\mathbf{F}^{-1}\mathbf{F}^{-T}\frac{1}{\alpha\kappa}\nabla_{\mathbf{X}} p_\beta) = J q_\beta; \tag{16}$$

using the complementary relation (1), and summing the two equations above, gives us

$$\frac{DJ}{Dt} - \nabla_{\mathbf{X}} \cdot (J\mathbf{F}^{-1}\mathbf{F}^{-T}\frac{1}{\alpha\kappa}\nabla_{\mathbf{X}} p_\beta) = 0 \qquad \text{in } \Omega_0 \times (0, T]. \tag{17}$$

For the Lagrangian balance of linear momentum, following the same steps as in the Eulerian case we obtain

$$-\nabla_{\mathbf{X}} \cdot \mathbf{P} = 0 \qquad \text{in } \Omega_0 \times (0, T],$$

where

$$\mathbf{P} = J\mathbf{T}\mathbf{F}^{-T}, \tag{18}$$

is the first Piola-Kirchhoff stress tensor, and $\mathbf{T}$ is the total Cauchy stress tensor (the stress of the mixture) in the reference configuration.

Note that the use of the Lagrangian setting allows us to consider the cell phase as a solid. Regarding the mechanochemical coupling, we adopt the assumption of active stress. In this case the microscopically generated active stresses of the mixture are considered as an additive contribution to the total stress. In a simplified rheological model, the active stress formalism corresponds to considering a parallel arrangement of a passive element and a newly introduced active element [29]. We decompose the first Piola–Kirchhoff stress tensor into

$$\mathbf{P} = \mathbf{P}_\alpha + \mathbf{P}_\beta + \mathbf{P}_{\text{active}}, \tag{19}$$

where $\mathbf{P}_\alpha$ is the effective solid stress for hyperelastic materials. We have

$$\mathbf{P}_\alpha = \frac{\partial \mathscr{W}}{\partial \mathbf{F}},$$

where $\mathscr{W}$ is a strain energy density depending on $\mathbf{F}$. For the specific case of Neo-Hookean poroelastic solids with material parameters $\mu_\alpha, \lambda_\alpha$, we obtain the following form for the effective first Piola–Kirchhoff stress tensor

$$\mathbf{P}_\alpha = \mu_\alpha(\mathbf{F} - \mathbf{F}^{-T}) + \lambda_\alpha J(J-1)\mathbf{F}^{-T}.$$

The stress due to the fluid phase and to the active mass change are, respectively

$$\mathbf{P}_\beta = -p_\beta J\mathbf{F}^{-T},$$

and

$$\mathbf{P}_{\text{active}} = -\alpha\Sigma(\alpha)J\mathbf{F}^{-T}. \tag{20}$$

In general, the active component of stress can depend on a set of phenomenological or physiologically relevant parameters that describe, for example, the state of a population of cells. This is precisely what is added in (20).

Remark 2.1. A more adequate description of growth in the Lagrangian framework is the multiplicative decomposition of the deformation gradient into a pure growth deformation tensor and an elastic rearrangement deformation $\mathbf{F} = \mathbf{F}_e\mathbf{F}_g$ (see, e.g., [21,26]). In such a case, $\mathbf{F}_g$ is determined from a growth factor $g(\alpha,t)$ whose evolution is dictated to preserve (15). We instead adopt an active stress approach which is much simpler to relate with the constitutive equation used for the linear elastic case in Eulerian coordinates.

Note that the conservation of angular momentum is also included, and it is encoded in the relation $\mathbf{P}\mathbf{F}^T = \mathbf{F}\mathbf{P}^T$.

In summary, we get the following initial-boundary value problem for the multiphase growth model in Lagrangian form

$$\frac{D}{Dt}(\alpha J) = Jq_\alpha(\alpha,C), \qquad\qquad \text{continuity of phase } \alpha$$

$$\frac{D}{Dt}(J) - \nabla_{\mathbf{X}}\cdot(\frac{J}{\alpha\kappa}\nabla_{\mathbf{X}}p_\beta) = 0, \qquad\qquad \text{continuity of the mixture}$$

$$\nabla_X\cdot\mathbf{P} = 0, \qquad\qquad \text{equation of motion for the mixture}$$

$$\mathbf{P} = \frac{\partial\mathscr{W}}{\partial\mathbf{F}} - p_\beta J\mathbf{F}^{-T} - \alpha\Sigma(\alpha)J\mathbf{F}^{-T}, \quad \text{constitutive equation}$$

$$-\nabla_{\mathbf{X}}\cdot(J\mathbf{F}^{-1}\mathbf{F}^{-T}\nabla_{\mathbf{X}}C) = Jq_C(\alpha,C). \qquad\qquad \text{continuity of oxygen}$$

To close the set of equations we need to provide suitable initial data and boundary conditions. We suppose that the system is initially at rest and with a given initial distribution of cells

$$\alpha(0) = \alpha_0, \quad d_\alpha(0) = 0 \quad \text{in } \Omega_0. \tag{21}$$

Boundary conditions depend on the specific case under consideration in the following sections. For the mixture we assume general mixed-loading boundary conditions including displacement essential conditions

$$d_\alpha = \hat{d}_0 \qquad \text{on } \partial\Omega_0^D \times (0,T],$$

and natural boundary conditions in the Lagrangian setting

$$\mathbf{P}\mathbf{N}_0 = \hat{\imath}_0 \qquad \text{on } \partial\Omega_0^N \times (0,T],$$

where $\partial\Omega_0^N$ and $\partial\Omega_0^D$ are two disjoint parts of the undeformed boundary, $\mathbf{N}_0$ is the unit vector outward normal to the body surface $\partial\Omega_0$ in the referential configuration, and $\hat{d}_0, \hat{\imath}_0$ are the prescribed Lagrangian displacement and traction on the boundary.

On the sub-boundary $\partial\Omega_0^N$ the oxygen concentration is maintained at a given value, whereas a flux is imposed on the remainder of the boundary

$$C = C_{\text{out}} \quad \text{on } \partial\Omega_0^N \times (0,T], \qquad J\mathbf{F}^{-1}\mathbf{F}^{-T}\nabla_{\mathbf{X}}C \cdot \mathbf{N}_0 = g_0 \quad \text{on } \partial\Omega_0^D \times (0,T].$$

2.3 Finite element discretisation for the Lagrangian model

The nonlinear weak form of the multiphase equations of motion collected in Section 2.2 can be established following a standard approach, that is, multiplying each field equation by a suitable test function, integrating over Ω_0, and invoking the divergence theorem (in tensorial and in vectorial form) whenever appropriate. For almost all $t > 0$, we look for $d_\alpha \in \mathbf{H}_D^1(\Omega_0) = \{v \in \mathbf{H}^1(\Omega) : v|_{\partial\Omega_0^D} = 0\}$, $p_\beta, C \in \mathrm{H}_N^1(\Omega_0) = \{s \in \mathrm{H}^1(\Omega) : s|_{\partial\Omega_0^N} = 0\}$, and $\alpha \in \mathrm{L}^2(\Omega_0)$, such that

$$\int_{\Omega_0} (\mathbf{P}_\alpha - [p_\beta + \alpha\Sigma(\alpha)]J\mathbf{F}^{-T}) : \nabla_{\mathbf{X}}\zeta \, dV_0 - \int_{\partial\Omega_0^N} J\mathbf{F}^{-T}\hat{\imath}_0 \cdot \zeta \, dS_0 = 0 \quad \forall \zeta \in \mathbf{H}_D^1(\Omega_0),$$
(22a)

$$\int_{\Omega_0} \frac{D}{Dt}(\alpha J)\eta \, dV_0 - \int_{\Omega_0} Jq_\alpha(\alpha,C)\eta \, dV_0 = 0 \quad \forall \eta \in \mathrm{L}^2(\Omega_0),$$
(22b)

$$\int_{\Omega_0} \frac{D}{Dt}(J)\psi \, dV_0 + \int_{\Omega_0} \frac{J}{\alpha\kappa}\mathbf{F}^{-1}\mathbf{F}^{-T}\nabla_{\mathbf{X}}p_\beta \cdot \nabla_{\mathbf{X}}\psi \, dV_0 = 0 \quad \forall \psi \in \mathrm{H}_N^1(\Omega_0),$$
(22c)

$$\int_{\Omega_0} J\mathbf{F}^{-1}\mathbf{F}^{-T}\nabla_{\mathbf{X}}C \cdot \nabla_{\mathbf{X}}\varphi \, dV_0 - \int_{\Omega_0} Jq_C(\alpha,C)\varphi \, dV_0 = 0 \quad \forall \varphi \in \mathrm{H}_N^1(\Omega_0).$$
(22d)

In order to define a Galerkin finite element method we denote by $\{\mathscr{T}_h\}_{h>0}$ a shape-regular family of partitions of $\bar{\Omega}_0$, conformed by triangles K of diameter h_K, with mesh size $h := \max\{h_K : K \in \mathscr{T}_h\}$. Given an integer $k \geq 1$ and a subset S of $\mathbb{R}^2$, by $\mathbb{P}_k(S)$ we will denote the space of polynomial functions defined locally in S and being of total degree up to k. Let us also denote by $b_K := \varphi_1\varphi_2\varphi_3$ a $\mathbb{P}_3$ bubble function in K, where $\varphi_1, \varphi_2, \varphi_3$ are the barycentric coordinates of the triangle K. Then the finite-dimensional subspaces for cell displacement $\mathbf{V}_h \subseteq \mathbf{H}_D^1(\Omega_0)$, porous
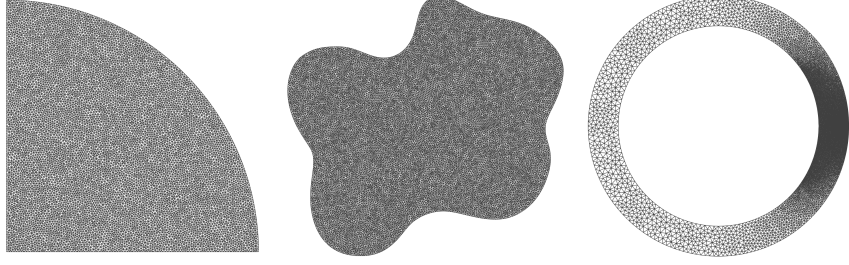
Fig. 1: Samples of unstructured triangular meshes generated for the tumour growth and plaque formation applications.

fluid pressure and oxygen $Q_h \subseteq H^1_N(\Omega_0)$, and solid phase volume fraction $R_h \subseteq L^2(\Omega_0)$ are defined, respectively, as follows

$$\mathbf{V}_h := \{\boldsymbol{\zeta}_h \in C(\overline{\Omega_0}) : \boldsymbol{\zeta}_h|_K \in [\mathbb{P}_1(K) \oplus \mathrm{span}\{b_K\}]^2 \ \forall K \in \mathscr{T}_h, \ \boldsymbol{\zeta}_h|_{\partial \Omega_0^D} = 0\},$$

$$Q_h := \{\psi_h \in C(\overline{\Omega_0}) : \psi_h|_K \in \mathbb{P}_1(K), \ \forall K \in \mathscr{T}_h, \ \psi_h|_{\partial \Omega_0^N} = 0\}, \tag{23}$$

$$R_h := \{\eta_h \in C(\overline{\Omega}) : \eta_h|_K \in \mathbb{P}_1(K), \ \forall K \in \mathscr{T}_h\}.$$

The pair $(\mathbf{V}_h, R_h)$ is the well-known MINI-element, which is inf-sup stable in the context of saddle-point Stokes equations in their usual velocity-pressure formulation [14].

Next we partition the interval $[0, t_{\text{final}}]$ into N evenly spaced non-overlapping sub-intervals of fixed length Δt and apply a time semi-discretisation of (22a) using the unconditionally stable, backward Euler's method. Further details on the discretisation and its suitability in solving the equations of motion are omitted here and we simply refer to, e.g., [5, 39].

2.4 Numerical results

In this section we present numerical simulations conducted with algorithms implemented using the open source finite element library FEniCS [1]. Sample codes (including meshes) are available from the public repository
https://github.com/ruizbaier/MATRIX_MultiphaseTissueModelling.
A fixed tolerance of 10^{-6} is used on the residuals for the convergence criterion of the Newton-Raphson iterative algorithm, and all the linear systems emanating from the discretisation of the tangent systems are solved with the direct method MUMPS. The three meshes used in our studies were generated with the library Gmsh [20] (see Figure 1).

2.4.1 Radial growth on a quarter disk

In our first set of simulations a tumour domain is considered as a unit disk. Only a quarter of the domain is taken into account. On the straight segments of the boundary we impose sliding conditions

$$d_\alpha \cdot \mathbf{N}_0 = 0 \qquad \text{on} \quad \partial \Omega_0^D \times (0, T].$$

For this example the time step is fixed to $\Delta t = 0.5$ and the system is evolved until $t_{\text{end}} = 60$ (adimensional time units). The parameter values are taken to be (see for example, [17])

$$\alpha_{\min} = \alpha_0 = \alpha^* = 0.8, \quad \mu_\alpha = C_{\text{out}} = k = 1, \quad \lambda_\alpha = p_\beta^{\text{out}} = \hat{Q}_1 = 0,$$
$$s_1 = s_4 = 10, \quad s_2 = s_3 = Q = 0.5,$$

where we note that permeability, diffusivity, and active stress are isotropic. In Figure 2 we portray snapshots of the oxygen tension plotted on the deformed configuration (which indicates domain growth). As the tumour grows larger, there is less oxygen available at the tumour 'centre' (the region furthest away from the free boundary). Once the oxygen concentration is below approximately 0.3, a necrotic core forms. From Figure 2, we observe that a necrotic core forms shortly after $t = 40$. In the necrotic core, (viable) tumour cells are replaced with necrotic material. The volume of tumour cells remains lower within the necrotic core (see the lighter region in the α snapshot at $t = 60$ in Figure 2), before rapidly increasing across the boundary between the necrotic core and the remainder of the tumour, then increasing linearly to the free boundary.

2.4.2 Progression of a glioblastoma

We simulate tumour growth in free suspension and therefore for this case we include pure traction boundary conditions with $\hat{t}_0 = 0$. In this situation we are required to remove rigid motions from the set of admissible displacement solutions. This is done using a Lagrange multiplier approach (imposing orthogonality with respect to the space of rigid motions; see for example, [30]). We employ here the same parameters as in the previous subsection.

The top row of Figure 3 depicts the volume fraction of cells on the deformed configuration, showing also the directions of displacement. These arrows confirm a radial growth imposed by the isotropic active stress distribution. In addition, we observe that at early times oxygen levels are everywhere sufficiently high to enable cell proliferation and therefore the tumour cell grows monotonically. The bottom row shows, for the time $t = 100$, the oxygen distribution and the magnitude of the first Piola–Kirchhoff stress tensor (19). From this we note a higher accumulation of stress near the reentrant boundaries of the tumour. We also note that the range of values for α and C vary considerably to the quarter-disk case. Over 100 time units, the
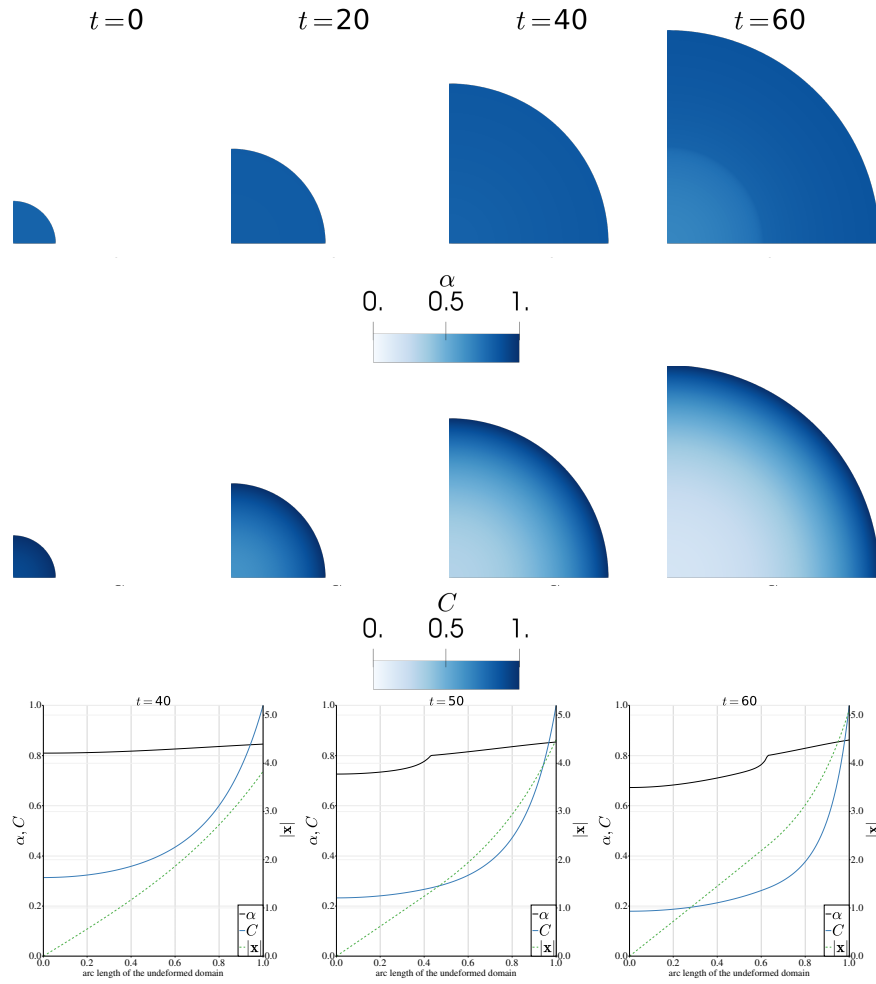
Fig. 2: Snapshots of the time evolution of cell volume fraction (top) and oxygen tension (middle row), plotted on the deformed configuration at times $t = 0, 20, 40, 60$ (adimensional units). The bottom row shows plots of α, C and the magnitude of the current position x along the centre line of the domain (at an angle of $45°$), for three times ($t = 40, 50, 60$).

concentration of oxygen never drops below 0.8 anywhere within the glioblastoma, even at the centre, and therefore a necrotic core never forms. Contrast this with the quarter-disk, where a necrotic core forms not long after $t = 40$ time units.

Next steps for this case study are including anisotropy and heterogeneity, not only in the active stress contribution, but also in the permeability parameter κ. For
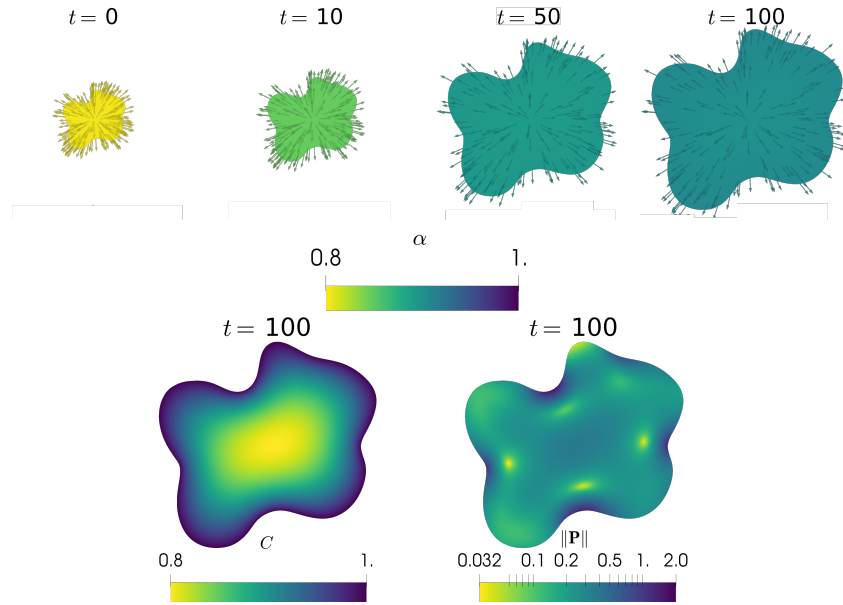
Fig. 3: Top: Snapshots of the time evolution of cell volume fraction, plotted on the deformed configuration at times $t = 0, 10, 50, 100$ (adimensional units). Arrows represent the displacement of the surface. Bottom: concentration of oxygen and magnitude of total stress at the final time $t = 100$. Note the log-scale on the magnitude of total stress. Shape based on [16, 19].

permeability we can use the same medical images employed to generate contours and meshes.

3 Model for plaque development

The mechanisms used in the modelling of tumour growth in Section 2, see also [3, 11], can serve as a starting point for formulating two-phase models for an early stage atherosclerotic plaque. The model that we develop herein follows [41, 42] and assumes that all cells coexist in a mixture medium where proteins diffuse. To capture the evolution of the plaque, we consider the region occupied by the plaque and its surroundings as a moving boundary domain. In the mixture we consider two phases: a macrophage phase (whose quantities are labelled with the subscript m) denoting its volume fraction also m, and a second phase (whose quantities are labelled with the subscript n), with volume fraction n, comprising foam cells, apoptotic and necrotic material, and other material such as extracellular matrix (which we henceforth refer to as necrotic material). We assume that there are no voids (the mixture is fully

saturated, with $n + m = 1$). We also include an equation for chemically modified low density lipoproteins (modLDL), whose concentration is denoted by l.

We first present the general framework. The equations of mass balance for the two phases gives:

$$\frac{\partial n}{\partial t} + \nabla_x \cdot (nu_n) = q_n, \tag{1a}$$

$$\frac{\partial m}{\partial t} + \nabla_x \cdot (mu_m) = q_m, \tag{1b}$$

where u_n and u_m are the velocities in the macrophage and necrotic phases, and q_n and q_m represent the rate of change in volume fractions for the macrophage and necrotic phases. Both phases are assumed incompressible.

Conservation of mass for modLDL is modelled with the following equation that considers advection in both phases, Fickian diffusion, and a sink term:

$$\frac{\partial l}{\partial t} + \nabla_x \cdot (l\hat{u} - D_l \nabla_x l) = q_l, \tag{2}$$

where $\hat{u} = mu_m + nu_n$ is the average velocity of the mixture, D_l is the intrinsic diffusivity of modLDL (assumed isotropic) and q_l is the rate of removal of modLDL by macrophages. Here we take

$$q_n = -q_m = k_m lm, \quad q_l = -k_l lm, \tag{3}$$

where we adopt a simple mass-action form for the phagocytic consumption of modLDL by macrophages (with k_l, k_m positive constants), although we note that more complicated forms could be considered. We also assume here that macrophages die of necrosis soon after becoming foam cells due to the impairment of normal apoptotic pathways, and that macrophages do not ingest necrotic material [7].

Conservation of momentum is assumed in both phases, neglecting inertial effects (which is justified by the timescales of cell growth and proliferation), leading to:

$$-\nabla_x \cdot (n\sigma_n) = \mathbf{b}_n, \tag{4a}$$

$$-\nabla_x \cdot (m\sigma_m) = \mathbf{b}_m, \tag{4b}$$

where σ_m and σ_n are the Cauchy stress tensors in the macrophage and necrotic phases, and $\mathbf{b}_m$ and $\mathbf{b}_n$ are the net sources of momentum in each phase. Assuming that there are no external momentum sources, we simply take $\mathbf{b}_m = -\mathbf{b}_n$ and consider that interaction forces only include a Darcy-type drag term:

$$\mathbf{b}_n = bn(1-n)(u_m - u_n).$$

Next, we supply the form of stresses in the necrotic and macrophage phases. We simply consider constitutive laws including an hydrostatic and a viscous contribution, giving:
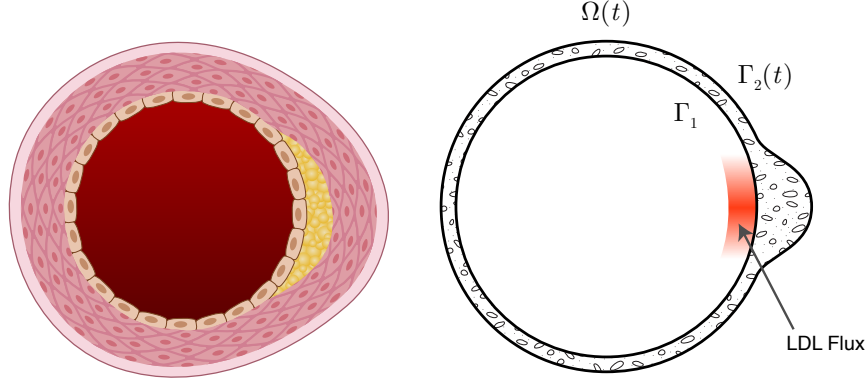
Fig. 1: Left: Cross-section of an artery. The pink cells are smooth muscle cells, the beige cells are endothelial cells, the yellow region shows the necrotic core and the red region is the lumen. Right: Model schematic.

$$\sigma_n = -p_n\mathbf{I} + 2\mu_n\varepsilon(u_n) + \lambda_n(\nabla \cdot u_n)\mathbf{I}, \tag{5a}$$

$$\sigma_m = -p_m\mathbf{I} + 2\mu_m\varepsilon(u_m) + \lambda_m(\nabla \cdot u_m)\mathbf{I}, \tag{5b}$$

where p_n and p_m are the pressures in the nectrotic and macrophage phases, μ_n and μ_m and λ_n and λ_m are the shear and bulk viscosity coefficients in the two phases. We further assume that the pressure difference between the macrophage and necrotic phases contributes to macrophage movement:

$$p_m = p_n + \Sigma,$$

and we take a form for the capillary pressure depending only on the volume fraction of the macrophage phase and the concentration of modLDL. This term is assumed to characterise the chemotaxis of macrophages towards higher levels of modLDL:

$$\Sigma(l,m) = \frac{A}{1 + Bl^k}, \tag{6}$$

where A, B and k are positive constants. These terms adopt the structure used in, e.g., [33].

For spatial domain $\Omega(t)$ we consider a cross-section through the artery wall, transverse to the direction of blood flow. Early and mid-stage plaque formation is observed to cause outward remodelling of the artery wall, where the radius of the lumen is preserved. We therefore take the inner endothelial boundary Γ_1 to be fixed. The outer boundary $\Gamma_2(t)$ separates the intima from the layers of muscle cells supporting the artery, and we assume that this boundary may vary with time (see a sketch of the geometry and boundary configuration in Figure 1).

We impose the following flux-type boundary conditions on the inner endothelial boundary:

$$\left(-\nabla_x l + l\hat{u}\right) \cdot n = \Psi_l \quad \text{on } \Gamma_1, \tag{7a}$$

$$mu_m \cdot n = \Psi_m l \quad \text{on } \Gamma_1, \tag{7b}$$

$$nu_n \cdot n = 0 \quad \text{on } \Gamma_1. \tag{7c}$$

Here, Ψ_l is the rate of LDL deposition in the artery wall, which will be localised over a specific region (for example, a particular angle). The presence of modLDL will stimulate macrophage recruitment, where the macrophage influx $mu_m|_{\Gamma_1} \cdot n$ is proportional to the concentration of l near the endothelium. Note that this is an essential part of the model as it represents the only contribution that will actively modify the behaviour of the plaque.

3.1 Simplification to one-dimensional geometry

In one dimension the model can be written as follows

$$\frac{\partial n}{\partial t} + \frac{\partial}{\partial x}(nu_n) = k_n lm, \tag{8a}$$

$$\frac{\partial}{\partial x}(mu_m + nu_n) = 0, \tag{8b}$$

$$\frac{\partial l}{\partial t} + \frac{\partial}{\partial x}\left(l\hat{u} - \frac{\partial l}{\partial x}\right) = k_l lm \text{ where } \hat{u} = nu_n + mu_m, \tag{8c}$$

$$-\frac{\partial}{\partial x}\left(n\left(-p_n + \mu_n\frac{\partial u_n}{\partial x} + \lambda_n\frac{\partial u_n}{\partial x}\right)\right) = b_n n(1-n)(u_m - u_n), \tag{8d}$$

$$-\frac{\partial}{\partial x}\left(m(-p_n - \Sigma(l,m) + \mu_m\frac{\partial u_m}{\partial x} + \lambda_m\frac{\partial u_m}{\partial x})\right) = -(b_n n(1-n)(u_m - u_n)), \tag{8e}$$

$$\left(-\frac{\partial l}{\partial x} + l\hat{u}\right)\Bigg|_{x=0} = \Psi_l, \tag{8f}$$

$$mu_m|_{x=0} = \Psi_m l|_{x=0}, \tag{8g}$$

$$nu_n|_{x=0} = 0, \tag{8h}$$

while the boundary conditions on the outer layer become:

$$m(u_m - L')|_{x=L} = n(u_n - L')|_{x=L} = l(u_l - L')|_{x=L} = 0. \tag{9}$$

For numerical purposes, we scale the spatial domain using $\xi = \frac{x}{L(t)}$ which then gives:

$$\frac{\partial n}{\partial t} - \frac{\xi}{L(t)}L'(t)\frac{\partial n}{\partial \xi} + \frac{1}{L(t)}\frac{\partial}{\partial \xi}(nu_n) = k_m lm, \tag{10a}$$

$$\frac{\partial l}{\partial t} - \frac{\xi}{L(t)}L'(t)\frac{\partial l}{\partial \xi} + \frac{1}{L(t)}\frac{\partial}{\partial \xi}\left(l\hat{u} - \frac{1}{L(t)}\frac{\partial l}{\partial \xi}\right) = -k_l lm. \tag{10b}$$

Implementing this model numerically and comparing to atherosclerotic plaque formation data is left for future work.

4 Discussion

This paper generalises the tumour growth model of Breward *et al.* [9] into general geometries and shows numerical solutions for the two-dimensional case using finite element variational formulations of the system. Our findings are consistent with previous work; however, we have used a different approach that can handle different geometries with relative ease. Given the current assumptions of the model the domain grows uniformly, and therefore the power of this technique is not fully realised. Extensions of this work could consider anisotropic stress and heterogeneous diffusivity and permeability to explore the effects of different geometries.

We additionally hypothesise a two-phase model for early atherosclerotic plaque formation. This work aims to complement the existing literature on late stage plaque behaviour [41, 42]. We leave the exploration of the numerical solution for future work. We note that to better understand early plaque formation it would be beneficial to separate the necrotic material phase further into its component parts. For example, formulating a three (or more) phase model to incorporate the difference between foam cells and apoptotic and necrotic material.

Acknowledgements

References

1. M. S. ALNÆS, J. BLECHTA, J. HAKE, A. JOHANSSON, B. KEHLET, A. LOGG, C. RICHARDSON, J. RING, M. E. ROGNES, AND G. N. WELLS, *The FEniCS Project Version 1.5*, Arch. Numer. Softw., 3 (2015), pp. 9–23.
2. D. AMBROSI AND S. PEZZUTO, *Active stress vs. active strain in mechanobiology: Constitutive issues*, Journal of Elasticity, 107 (2012), pp. 199–212.

3. D. AMBROSI AND L. PREZIOSI, *On the closure of mass balance models for tumor growth*, Mathematical Models and Methods in Applied Sciences, 12 (2002), pp. 737–754.

4. R. P. ARAUJO AND D. S. MCELWAIN, *A history of the study of solid tumour growth: the contribution of mathematical modelling*, Bulletin of Mathematical Biology, 66 (2004), pp. 1039–1091.

5. N. BARNAFI, B. GÓMEZ-VARGAS, W. D. J. LOURENÇO, R. F. REIS, B. M. ROCHA, M. LOBOSCO, R. RUIZ-BAIER, AND R. WEBER DOS SANTOS, *Finite element methods for large-strain poroelasticity/chemotaxis models simulating the formation of myocardial oedema*, Journal of Scientific Computing, 92 (2022), pp. e92(1–40).

6. L. BERGER, R. BORDAS, D. KAY, AND S. TAVENER, *A stabilized finite element method for finite-strain three-field poroelasticity*, Computational Mechanics, 60 (2017), pp. 51–68.

7. Y. V. BOBRYSHEV, E. A. IVANOVA, D. A. CHISTIAKOV, N. G. NIKIFOROV, AND A. N. OREKHOV, *Macrophages and their role in atherosclerosis: pathophysiology and transcriptome analysis*, BioMed Research International, 2016 (2016).

8. D. BOFFI, F. BREZZI, AND M. FORTIN, *Mixed Finite Element Methods and Applications*, vol. 1, Springer-Verlag, Berlin, 2013.

9. C. BREWARD, H. BYRNE, AND C. LEWIS, *The role of cell-cell interactions in a two-phase model for avascular tumour growth*, Journal of Mathematical Biology, 45 (2002), pp. 125–152.

10. C. J. BREWARD, H. M. BYRNE, AND C. E. LEWIS, *A multiphase model describing vascular tumour growth*, Bulletin of Mathematical Biology, 65 (2003), pp. 609–640.

11. H. BYRNE AND L. PREZIOSI, *Modelling solid tumour growth using the theory of mixtures*, Mathematical Medicine and Biology: A Journal of the IMA, 20 (2003), pp. 341–366.

12. H. M. BYRNE, *12.1 continuum models of avascular tumor growth*, in Mathematics and Life Sciences, De Gruyter, 2012, pp. 279–312.

13. H. M. BYRNE, J. R. KING, D. S. MCELWAIN, AND L. PREZIOSI, *A two-phase model of solid tumour growth*, Applied Mathematics Letters, 16 (2003), pp. 567–573.

14. A. CIONCOLINI AND D. BOFFI, *The MINI mixed finite element for the Stokes problem: An experimental investigation*, Comput. Math. Appl., 77 (2019), pp. 2432–2446.

15. O. COUSSY, *Poromechanics*, John Wiley & Sons, 2004.

16. V. CRISTINI AND J. LOWENGRUB, *Multiscale modeling of cancer: an integrated experimental and mathematical modeling approach*, Cambridge University Press, 2010.

17. J. DRONIOU, J. A. FLEGG, AND G. C. REMESAN, *Numerical solution of a two dimensional tumour growth model with moving boundary*, Journal of Scientific Computing, 85 (2020), pp. 1–31.

18. H. B. FRIEBOES, F. JIN, Y.-L. CHUANG, S. M. WISE, J. S. LOWENGRUB, AND V. CRISTINI, *Three-dimensional multispecies nonlinear tumor growth—ii: tumor invasion and angiogenesis*, Journal of Theoretical Biology, 264 (2010), pp. 1254–1278.

19. H. B. FRIEBOES, J. S. LOWENGRUB, S. WISE, X. ZHENG, P. MACKLIN, E. L. BEARER, AND V. CRISTINI, *Computer simulation of glioma growth and morphology*, Neuroimage, 37 (2007), pp. S59–S70.

20. C. GEUZAINE AND J. F. REMACLE, *Gmsh: A 3-D finite element mesh generator with built-in pre- and post-processing facilities*, Int. J. Numer. Methods Eng., 79 (2009), pp. 1309–1331.

21. A. GORIELY AND R. VANDIVER, *On the mechanical stability of growing arteries*, IMA J. App. Math., 75 (2010), pp. 549–570.

22. J. GREEN, J. WHITELEY, J. OLIVER, H. BYRNE, AND S. WATERS, *Pattern formation in multiphase models of chemotactic cell aggregation*, Mathematical Medicine and Biology: A Journal of the IMA, 35 (2018), pp. 319–346.

23. H. GREENSPAN, *Models for the growth of a solid tumor by diffusion*, Studies in Applied Mathematics, 51 (1972), pp. 317–340.

24. ———, *On the growth and stability of cell cultures and solid tumors*, Journal of Theoretical Biology, 56 (1976), pp. 229–242.

25. M. HUBBARD AND H. BYRNE, *Multiphase modelling of vascular tumour growth in two spatial dimensions*, Journal of Theoretical Biology, 316 (2013), pp. 70–89.

26. G. W. JONES AND S. J. CHAPMAN, *Modeling growth in biological materials*, SIAM Rev., 54 (2012), pp. 52–118.

27. A. KAROLAK, D. A. MARKOV, L. J. MCCAWLEY, AND K. A. REJNIAK, *Towards personalized computational oncology: from spatial models of tumour spheroids, to organoids, to tissues*, Journal of The Royal Society Interface, 15 (2018), p. 20170703.

28. N. KIDA AND Y. MORISHITA, *Continuum mechanical modeling of developing epithelial tissues with anisotropic surface growth*, Finite Elem. Anal. Des., 144 (2018), pp. 49–60.

29. T. KLOTZ, C. BLEILER, AND O. RÖHRLE, *A physiology-guided classification of active-stress and active-strain approaches for continuum-mechanical modeling of skeletal muscle tissue*, Frontiers in Physiology, 12 (2021).

30. M. KUCHTA, K.-A. MARDAL, AND M. MORTENSEN, *On the singular neumann problem in linear elasticity*, Numerical Linear Algebra with Applications, 26 (2019), p. e2212.

31. E. KUHL, *Growing matter: A review of growth in living systems*, J. Mech. Behav. Biomed. Mater., 29 (2014), pp. 529–543.

32. K. LANDMAN AND C. PLEASE, *Tumour dynamics and necrosis: surface tension and stability*, Mathematical Medicine and Biology: A Journal of the IMA, 18 (2001), pp. 131–158.

33. G. LEMON, J. R. KING, H. M. BYRNE, O. E. JENSEN, AND K. M. SHAKESHEFF, *Mathematical modelling of engineered tissue growth using a multiphase porous flow mixture theory*, Journal of Mathematical Biology, 52 (2006), pp. 571–594.

34. X. LI, Z. LIU, R. W. LEWIS, AND K. SUZUKI, *Mixed finite element method for saturated poroelastoplastic media at large strains*, International Journal for Numerical Methods in Engineering, 57 (2003), pp. 875–898.

35. J. METZCAR, Y. WANG, R. HEILAND, AND P. MACKLIN, *A review of cell-based computational modeling in cancer biology*, JCO Clinical Cancer Informatics, 2 (2019), pp. 1–13.

36. R. J. MURPHY, A. P. BROWNING, G. GUNASINGH, N. K. HAASS, AND M. J. SIMPSON, *Designing and interpreting 4d tumour spheroid experiments*, Communications Biology, 5 (2022), pp. 1–11.

37. L. PREZIOSI AND A. TOSIN, *Multiphase modelling of tumour growth and extracellular matrix interaction: mathematical tools and applications*, Journal of Mathematical Biology, 58 (2009), pp. 625–656.

38. T. ROOSE, S. J. CHAPMAN, AND P. K. MAINI, *Mathematical models of avascular tumor growth*, SIAM Review, 49 (2007), pp. 179–208.

39. R. RUIZ-BAIER, *Primal-mixed formulations for reaction-diffusion systems on deforming domains*, Journal of Computational Physics, 299 (2015), pp. 320–338.

40. J. P. WARD AND J. KING, *Mathematical modelling of avascular-tumour growth*, Mathematical Medicine and Biology: A Journal of the IMA, 14 (1997), pp. 39–69.

41. M. G. WATSON, H. M. BYRNE, C. MACASKILL, AND M. R. MYERSCOUGH, *A two-phase model of early fibrous cap formation in atherosclerosis*, Journal of Theoretical Biology, 456 (2018), pp. 123–136.

42. ——, *A multiphase model of growth factor-regulated atherosclerotic cap formation*, Journal of Mathematical Biology, 81 (2020), pp. 725–767.

43. S. M. WISE, J. S. LOWENGRUB, H. B. FRIEBOES, AND V. CRISTINI, *Three-dimensional multispecies nonlinear tumor growth—i: model and numerical method*, Journal of Theoretical Biology, 253 (2008), pp. 524–543.